Available online at www.CivileJournal.org

Civil Engineering Journal

(E-ISSN: 2476-3055; ISSN: 2676-6957)

Vol. 10, No. 08, August, 2024

Load Capacity and Bending Strength of Double-Acting Friction Stir Welded AA6061 Hollow Panels

Nurul Muhayat [1], Muhammad Budi Utama [1], Ericha Dwi Wahyu Syah Putri [1], Eko Prasetya Budiana [1], Aditya Rio Prabowo [1], Yohanes P. D. S. Depari [2], Triyono [1*]

[1] *Department of Mechanical Engineering, Universitas Sebelas Maret, Surakarta, 57126, Indonesia.*

[2] *National Research and Innovation Agency of Republic Indonesia (BRIN), Jakarta Pusat 10340, Indonesia.*

Received 11 April 2024; Revised 18 July 2024; Accepted 25 July 2024; Published 01 August 2024

Abstract

Aluminum alloy hollow panels are essential components in both civil and mechanical structures, such as building floors or large vehicle platforms. They enhance rigidity while staying lightweight and conserving material volume. In its application, this panel must be joined using welding methods. One common issue encountered in aluminum welding is the formation of porosity defects. Solid-state welding methods like Friction Stir Welding (FSW) can be a solution to address this problem. The FSW joining process on hollow panels cannot be completed in one welding operation due to their thickness. The FSW process must be performed on both surfaces, which requires a relatively long time. Therefore, FSW needs to be developed into a Double-acting FSW that utilizes two tools simultaneously. These two tools introduce two sources of heat input, pressing force, and friction-stirring, resulting in a novel response that needs further research. This study delves into the impact of welding speed variations in Double-Acting FSW on the load capacity and bending strength of AA 6061 hollow panel joints. Welding speeds of 20, 30, and 40 mm/min were tested alongside rotational speed (1500 rpm), tilt angle (2°), and shoulder diameter (24 mm). It was discovered that reducing welding speed enhances both load capacity and bending strength. Notably, specimens welded at 20 mm/min exhibited a load capacity of 15.61 kN and bending strength of 52 MPa, highlighting the potential of slower speeds for superior weld performance.

Keywords: Hollow Panel; Aluminum Alloy; Double-Acting Friction Stir Welding; Welding Speed.

1. Introduction

In recent years, there has been a notable increase in the use of aluminum alloys as structural materials, mainly because of their beneficial properties. These include a high strength-to-weight ratio, ease of fabrication, good workability, sufficient flexibility, impressive thermal conductivity, high corrosion resistance, and an appealing natural appearance [1-3]. Consequently, a significant portion (25%) of global aluminum production is now directed towards the construction sector. The inherent ease of extrusion in aluminum alloys makes them highly adaptable as structural materials. This allows for the creation of intricate shapes, including complex cross-sections or hollow designs, which are suitable for structures that surpass the capabilities of traditional materials like concrete or steel. Their remarkable resistance to corrosion makes aluminum alloys particularly well-suited for use in marine environments. Such applications demand minimal surface protection and incur low maintenance costs. Furthermore, recent technological advancements, driven by sustainability and climate change mitigation efforts, have led to the development of innovative aluminum structural

* Corresponding author: triyono74@staff.uns.ac.id

http://dx.doi.org/10.28991/CEJ-2024-010-08-018

systems. These systems offer superior environmental and economic efficiency compared to their steel and concrete counterparts. However, one limitation of aluminum is its relatively low stiffness compared to steel, making it suitable for applications in the form of hollow panels. Hollow panels allow aluminum to meet stiffness requirements while maintaining a lightweight and low-volume structure [4]. In the fabrication, aluminum hollow panel structures necessitate welding processes. Metal Inert Gas (MIG) welding is a popular choice for aluminum welding due to its ease of operation, cost-effectiveness, and simplicity [5]. Nevertheless, a common issue encountered in aluminum welding is the formation of porosity defects, which is attributed to aluminum's high hydrogen gas (H2) solubility in its liquid state, decreasing significantly at room temperature.

Addressing the challenges posed by traditional fusion welding, solid-state welding methods such as Friction Stir Welding (FSW) offer promising solutions [6]. The FSW process circumvents the need to reach the material's melting point, thereby preventing the entry of hydrogen gas (H2) into the joint area. FSW utilizes a non-consumable tool that operates on the workpiece's surface while traversing the joint area. Compared to fusion welding, FSW can yield joints with improved microstructure and higher tensile strength. Additionally, the FSW process induces dynamic recrystallization in the grain structure, resulting in finer and denser grains [7]. However, FSW encounters difficulties when applied to thick materials due to limitations in tool size. To overcome this limitation, a modification of conventional FSW has been proposed by previous researchers. The differential double-shoulder friction stirs welding (DDS-FSW) technology, introduced by Liu et al. (2023), features a stir tool characterized by the separation of the upper and lower shoulders and pin, allowing independent control of the rotation direction and speed of the shoulders and pin. DDS-FSW has been shown to enhance the uniformity of temperature and microstructure of the joint [8-10]. Although this method is capable of homogenizing temperature across the thickness of the joined plate by utilizing two shoulders to generate heat on both sides of the plate surface, stirring is only performed on one side of the plate because the tool has only one pin. As a result, material stirring is uneven across the plate thickness, leading to inconsistent material flow and dynamic recrystallization rates. To refine this concept, this study proposes a new method known as Double-acting Friction Stir Welding (DA-FSW). This method involves the use of two rotational tools to join both sides simultaneously. Each of these tools has its own shoulder and pin section, working independently of each other, allowing for individual adjustment of welding parameters. In addition to improving DDS-FSW, DA-FSW also represents an advancement of the Double-side Friction Stir Welding (DS-FSW) technique. In DS-FSW, welding is initially performed on one side, necessitating a subsequent flip of the material for welding on the opposite side. However, this dual-welding approach prolongs the process time. Consequently, DS-FSW has evolved into DA-FSW, where two tools are employed simultaneously, enabling concurrent welding on both sides.

Friction Stir Welding (FSW) is a widely acknowledged technique for joining materials, with its effectiveness being heavily influenced by various parameters, notably welding speed [11]. These parameters play a pivotal role in determining both the mechanical properties and microstructure of the workpiece [12]. Notably, lower welding speeds in FSW can result in elevated heat generation, potentially leading to the formation of flash defects [13]. Conversely, an optimal welding speed can significantly enhance joint mechanical properties, including strength and hardness [14-16]. However, existing studies have shown that lower welding speeds may cause higher temperatures and smaller grain sizes, albeit with the potential drawback of reduced bond strength between metal components [13, 15]. Additionally, research by Liu et al. (2013) has highlighted the benefits of increasing welding speed, which reduces heat input and diminishes roughness in the welding area [15].

In the realm of Double-acting Friction Stir Welding (DA-FSW), employed for solid plates, both welding speed and tool rotation speed play critical roles in dictating microstructure evolution, hardness, and joint strength [17]. Furthermore, they influence factors such as fatigue behavior and corrosion rate [18, 19]. However, when considering the application of Double-acting Friction Stir Welding (DA-FSW) for hollow panels, characterized by their unique hollow structure, the dynamics shift. The heat generated by the friction of the tool within hollow panel components, such as the skin and fin, disperses more rapidly compared to solid plates. Consequently, there arises a pressing need for a more thorough evaluation of the parameters of Double-acting Friction Stir Welding (DA-FSW) specific to hollow panels. Although Hilmawan et al. (2024) have commenced such an evaluation, focusing on the impact of tool rotational speed on the microstructure evolution and mechanical properties of Double-acting Friction Stir Welded hollow panels [20], there remains a research gap in optimizing welding speed for achieving joints with high tensile strength [13].

Existing research has indeed shed light on the effects of welding speed in conventional FSW on joint quality. Nevertheless, the utilization of two tools in Double-acting FSW introduces dual sources of heat input—pressing force and friction-stirring—resulting in unique force and temperature distributions that can significantly influence plastic deformation and weld joint properties. This study aims to address this gap by investigating welding speed variations of 20 mm/min, 30 mm/min, and 45 mm/min in Double-acting Friction Stir Welding (DA-FSW). The comprehensive analysis of the observed physical and mechanical properties, encompassing microstructure, macrostructure, load capacity, and bending strength, will offer invaluable insights into the behavior of Double-acting FSW and its potential as an advanced welding technique for aluminum hollow panels. To present the answers to the issues in this study, four sections are outlined. Section 1 covers the introduction, encompassing the background, research gap, and novelty of the study. Section 2 details the research method, describing the conduct of this research, including the welding process, simulation process, and testing process. Section 3 focuses on the results and discussion, presenting the research data comprehensively and comparing it with previous research data to draw conclusions. The conclusion of the discussion results is presented in the final section, namely Section 4.

2. Material and Methods

The research activity consists of several stages: material preparation, setting up DAFSW machine equipment, preparing software, welding, simulation, characterizing welded joints, and discussion. These stages are outlined in a research flowchart depicted in Figure 1. The material utilized in this study was an extruded Aluminum Alloy AA6061 hollow panel, which exhibits a curvature profile as depicted in Figure 2. The joint configuration of hollow panel is illustrated in Figure 3 while the chemical composition is shown in Table 1. The tool's rotational speed and tilt angle were set constant at 1500 rpm and 2° respectively. These parameters were taken based on the previous studies [17-19]. This research involved three variations of welding speeds: 20 mm/min, 30 mm/min, and 40 mm/min. The selection of the welding speed range involves an initial research phase relying on trial and error. Based on these initial experiments, a welding speed of 20 mm/min represents the lowest speed capable of producing a welded joint, and a speed of 40 mm/min is the highest speed still resulting in a successful welded joint. Welding at speeds below 20 mm/min fails to create a joint, while speeds exceeding 40 mm/min lead to joint damage. The tool dimension parameter was characterized by a shoulder diameter of 24 mm, a pin diameter of 4 mm, and a pin length of 2.8 mm. Figure 4 illustrates the Double-acting Friction Stir Welding (DA-FSW) process applied to the hollow panel. Due to the relative position of tools and specimen, the upper tool is referred to as welding in the 1G welding position, while the lower tool is referred to as welding in the 4G welding position.

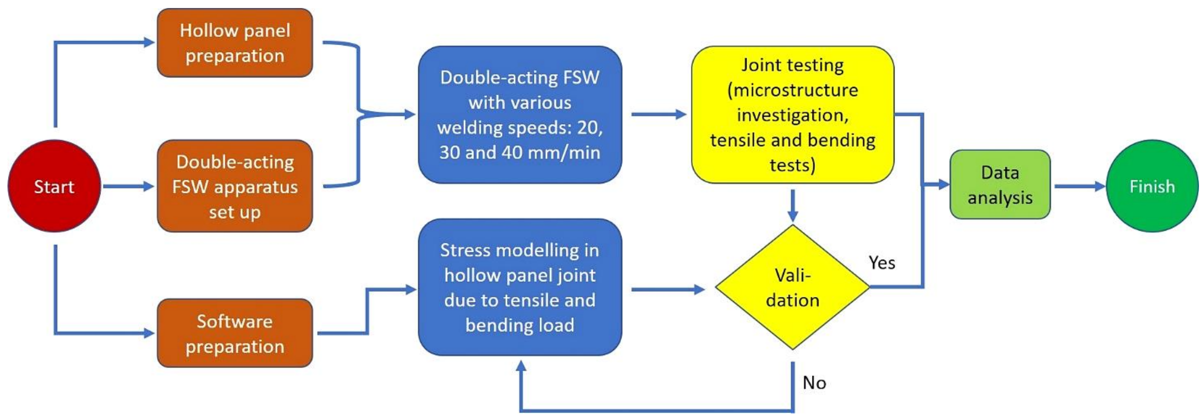

Figure 1. Flowchart of research activities

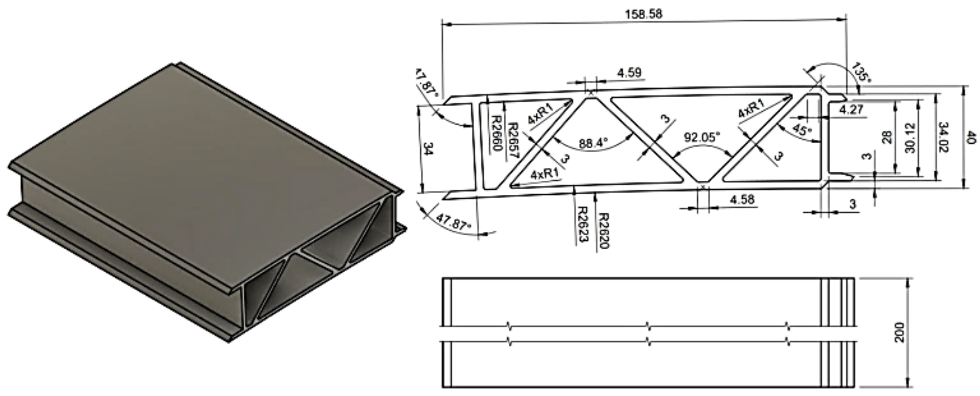

Figure 2. The dimension and profile of hollow panel (unit in mm)

Table 1. Chemical composition of Aluminum Alloy AA6061

Elements	Al	Fe	Cu	Mn	Mg	Zn	Cr	Ti
%wt	balance	0.21	0.00	0.01	0.56	0.01	0.00	0.02

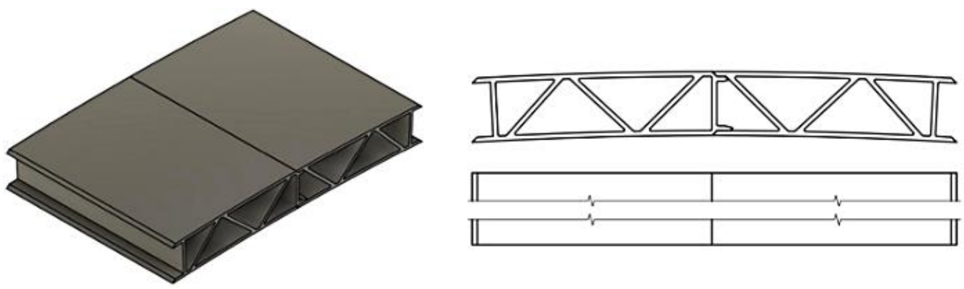

Figure 3. The joint configuration of hollow panel

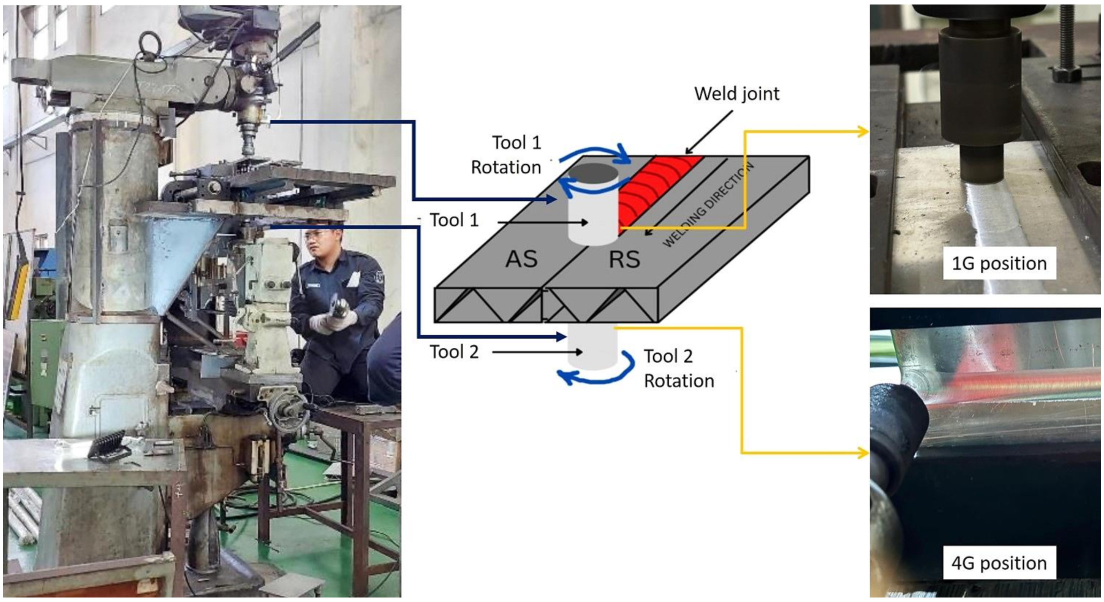

Figure 4. the Double-acting Friction Stir Welding (DA-FSW) process

Several tests were conducted on the DA-FSW hollow panel joints, including metallographic investigation, hardness, tensile, and bending tests. In the metallographic investigation, the observed surface was sandpapered, polished and etched. Weck's reagent (4 g $KMnO_4$, 1 g NaOH, and 100 mL H_2O) and Keller reagent (12 mL HF, 15 mL HCL, 25 mL HNO_3, and 80 mL H_2O) were used for revealing microstructure and macrostructure respectively. Hardness measurement was performed on all welding areas using the micro-Vickers method, adhering to the BN ISO 9015-1 standard. Tensile testing was implemented to observe the phenomena of joint fractures. During the tensile testing process, the backed support was applied to the clamped sections of an aluminum hollow panel to prevent any undesirable deformation of the test material [21]. This backed support plays a pivotal role in ensuring the continuous transmission of the force applied by the testing machine, leading to a gradual and controlled increase in the force exerted on the material [22].

The material was clamped on both sides and pulled with a load of 100 kN. The phenomena of cracks were also observed through bending tests, performed in accordance with the ISO 5173 standard. This testing involved a stress point in the 1G position with a 100 kN load and a 60 mm distance between supports. The tensile and bending tests performed on the extruded aluminum hollow panel joints are demonstrated in Figure 5. Simulations of tensile and bending tests under real conditions were also conducted using SAP software. It determines force direction in parts of hollow panel during loading, simulates the stress distribution and identifies the maximum stress. During the model creation process, precise definitions of the hollow panel structure's material properties and geometry were established using SAP2000. Key parameters, including Young's Modulus (E), density, and Poisson's ratio, were set at 68.9 GPa, 2.7x10^6 kg/mm^3, and 0.33, respectively. Faithfully representing the panel thickness and integrating any cutouts or holes into the model is essential. A mesh was generated and refined, particularly focusing on critical areas such as corners, holes, and regions prone to stress concentration. Considering a panel thickness of 3 mm, the mesh was aligned accordingly. Tensile or bending loads were applied to suitable nodes or elements during model loading, with an incremental load rate of 50 MPa/sec. The resulting stress magnitude adhered to design specifications. Furthermore, accounting for boundary conditions that may impact stress distribution within the structure is crucial. Special attention was given to points where deflection is constrained at supports.

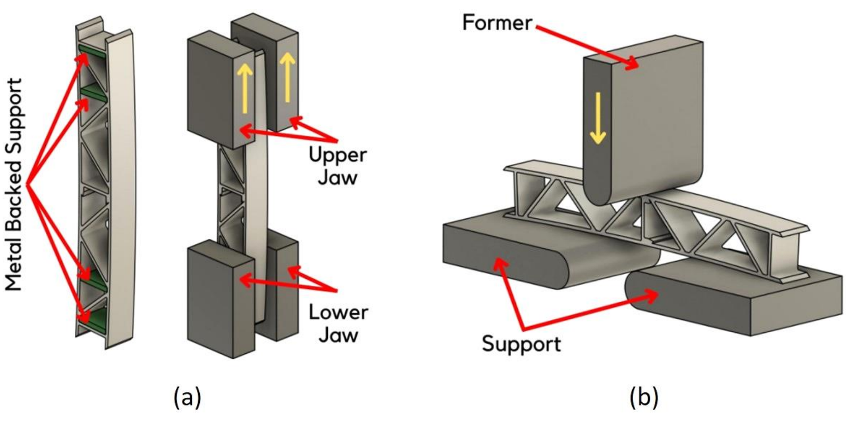

Figure 5. Mechanical testing: (a) tensile test (b) bending test

3. Results and Discussion

3.1. Weld Bead Appearance

Figure 5 offers a comprehensive view of how beads manifest on specimens crafted through Double-acting Friction Stir Welding (DA-FSW). Generally, this welding method seamlessly joins two surfaces of hollow panels in a single process. It's crucial to balance clamping and force control on both tools. An imbalance, where the force from tool 1 exceeds that from tool 2, results in increased plunge depth and flash defects on tool 2's welding surface, and vice versa. Upon closer scrutiny of Figure 6, specimens welded at a slower speed of 20 mm/min exhibit smoother bead surfaces and fewer defects compared to those welded at higher speeds. In low-speed welding, the heat generated from shoulder friction adequately softens the aluminum, facilitating an effective stirring process. Conversely, higher welding speeds lead to insufficient heat from shoulder friction, resulting in imperfect aluminum softening, less effective stirring, and rougher bead surfaces. Surface groove defects, identified by hollow lines on the welding surface, are one such defect related to heat generation [23, 24]. These lines stem from inadequate material flow. The longest surface groove defect, measuring 80 mm, was observed in specimens welded at a speed of 40 mm/min. Those welded at 30 mm/min and 20 mm/min hardly displayed any surface groove defects, and if present, they were minimal and usually occurred towards the end of the welding process. Moreover, Figure 5 reveals common defects in all specimens: pinholes and flash. These defects are inherent to every Friction Stir Welding (FSW) process. Flash defects arise when excessive heat input causes material in the joint path to peel off, pushing surrounding material outwards [25, 26]. Exit hole defects are imperfections occurring when the tool is lifted from the workpiece [27]. It's worth noting that these defects can be rectified using re-filling techniques [28].

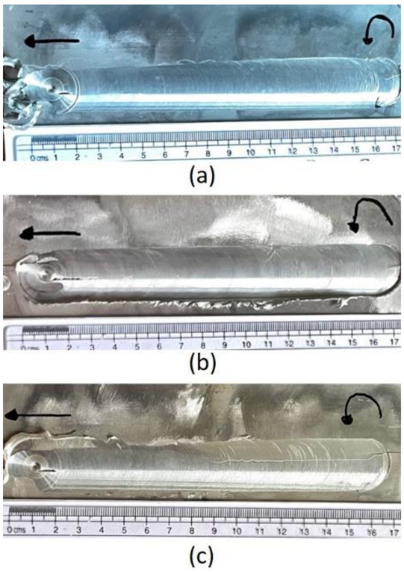

Figure 6. Bead appearance of specimen with welding speed of (a) 20 mm/min, (b) 30 mm/min and (c) 40 mm/min

Based on observations of macro structures, when comparing friction stir welding (FSW) results on solid plates to double-acting friction stir welding (DA-FSW) on hollow panel, it's clear that achieving optimal joints with DA-FSW requires significantly lower welding speeds. Conventional FSW on solid plates typically operates between 30-100 mm/min and reliably produces defect-free welds [14, 15]. Similarly, when using DA-FSW on solid plates, welding at a speed of 30 mm/min effectively bonds aluminum plates without defects [17-19]. However, when DA-FSW is applied to hollow panels, defects can still occur even at a speed of 30 mm/min due to insufficient heat input into the specimen. This deficiency arises from the distribution of welding heat during the frictional interaction between the tool and the workpiece, particularly within the structure of the hollow panel. Heat tends to disperse more readily into areas of hollow panel parts, such as fins and skins. This challenge is compounded by aluminum's high thermal conductivity. To generate enough heat to adequately soften the material, welding perforated panels requires more energy than welding solid plates, even if the plate thickness matches that of the fins or skins of the perforated panel. Consequently, to enhance heat energy generation, the welding speed for FSW on perforated panels must be slower than that used for solid plates.

3.2. Macrostructure and Microstructure Analysis

Figure 7 presents the results of macroscopic and microscopic examinations of DA-FSW specimens at different welding speeds. Notably, all specimens exhibit a consistent grain distribution pattern across various welding areas. The microstructural analysis delineated distinct characteristics in each zone of the welded joints. The Stir Zone (SZ) displayed the finest grains due to grain recrystallization induced by intense stirring action during welding [29]. This refinement enhances the joint's mechanical properties such as strength and ductility. Grain recrystallization in the SZ is triggered by elevated temperatures and frictional forces between the shoulder, pin, and the specimen surface. Moving to the Thermo-Mechanically Affected Zone (TMAZ), the grain size is coarser than the SZ but finer than the Heat Affected Zone (HAZ). The TMAZ experiences significant thermal and mechanical effects during welding but lacks the intense stirring action of the SZ, resulting in a less refined grain structure influenced by both heat and mechanical deformation. Conversely, the HAZ features larger grains primarily due to thermal effects without substantial mechanical deformation. The grain structure in the HAZ reflects the thermal history of the material, with grains growing larger due to heating without significant mechanical alteration. The grain size in the HAZ is mainly shaped by thermal aspects, rendering them finer than those in the Base Metal (BM).

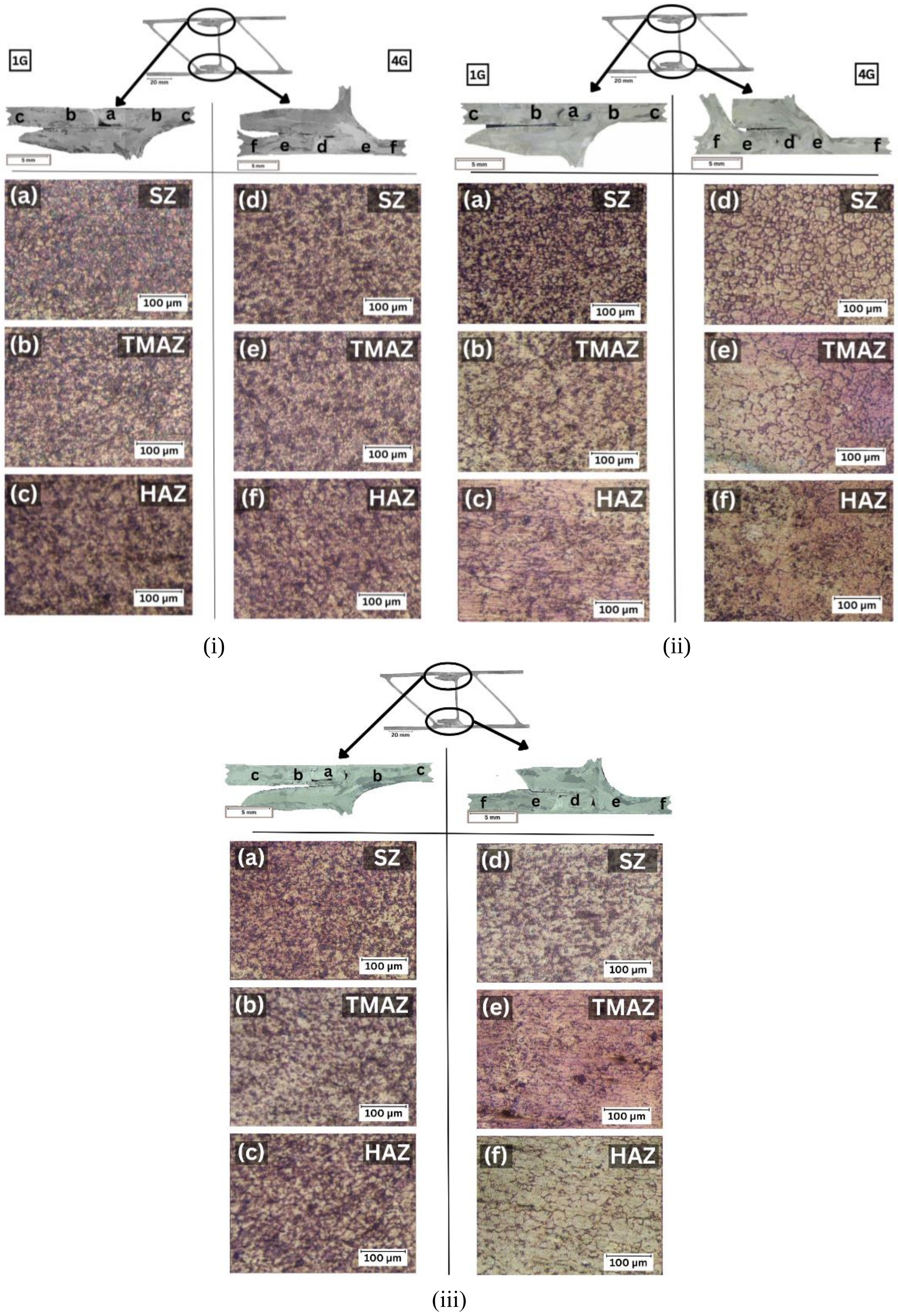

Figure 7. Macro and microstructure of SDFSW with welding speed of (i) 20 mm/min, (ii) 30 mm/min, and (iii) 40 mm/min where (a) SZ 1G, (b) TMAZ 1G, (c) HAZ 1G, (d) DXZ 4G, (e) TMAZ 4G, (f) HAZ 4G

To investigate the effects of welding speed on the microstructures of DA-FSW joints, a detailed comparison of Figures 7-i to 7-iii is essential. In this study, these figures respectively represent low welding speed (20 mm/min), medium welding speed (30 mm/min), and high welding speed (40 mm/min). It's worth noting that the categorization of welding speed in this study differs from that in Friction Stir Welding of solid plates, where a welding speed of 50 mm/min is considered low and 100 mm/min is considered high. Despite this discrepancy in numerical values, the observed trends in microstructure remain consistent. Low welding speeds in DA-FSW result in a more refined microstructure within the Stir Zone (SZ) due to prolonged stirring action (Figures 7-i(a) and 7-i(d)). Conversely, high welding speeds lead to coarser grains in the SZ due to reduced stirring time and less intense plastic deformation Figures 7-iii(a) and 7-iii(d)). Low welding speeds also allow for greater heat input and longer exposure to mechanical deformation, resulting in a more significant Thermo-Mechanically Affected Zone (TMAZ). This zone experiences both thermal and mechanical effects, influencing grain size and microstructure accordingly (Figure 7-i(b) and 7-i(e)). In contrast, high welding speeds produce a narrower TMAZ with less pronounced effects, as the shorter duration of heat and deformation exposure limits microstructural changes (Figure 7-iii(b) and 7-iii(e)). Moreover, low welding speeds typically result in a wider Heat Affected Zone (HAZ) due to prolonged exposure to elevated temperatures, leading to grain growth within this zone (Figure 7-i(c) and 7-i(f)). Conversely, high welding speeds produce a narrower HAZ with less heat input, minimizing the extent of grain growth (Figure 7-iii(c) and 7-iii(f)). The microstructure resulting from medium welding speeds exhibits characteristics between those observed at low and high welding speeds, as depicted in Figure 7-ii. This suggests a transitional behavior in grain size and microstructural features corresponding to varying welding speeds. Grain size is largely derived from factors such as heat input and strain rate. On the one hand, increasing heat input increases atomic diffusion, facilitating grain boundary movement and thereby causing the grain size to become coarser. On the other hand, high strain rates, associated with slower welding speeds, promote the nucleation process, thereby potentially fine-tuning the grain size [30]. These findings highlight the intricate relationship between welding speed and microstructural evolution in DA-FSW, underscoring the importance of optimizing welding parameters to achieve desired microstructural characteristics and mechanical properties.

Based on the macroscopic review, there are two main types of defects identifiable within the weld area of the Double-acting Friction Stir Welding (DA-FSW) joints: the tunnel defect and the kissing bond defect. However, it's notable that the size or magnitude of these defects varied based on the welding speed employed. The tunnel defect is essentially a void or cavity located just beneath the weld surface. This type of defect emerges due to an insufficient amount of plasticization of the material, often attributed to an inadequacy of heat input during the welding process [31, 32]. This means that when there's not enough heat to adequately soften the material, it fails to merge seamlessly, leading to the creation of this cavity. On the contrary, the kissing bond defect is identified by a partial residue within the weld joint which hasn't been fully amalgamated. This defect is signified by the presence of deformed grains at the interface of the Stirred Zone (SZ) and the Thermo-Mechanically Affected Zone (TMAZ) [33, 34]. The most common cause behind the formation of a kissing bond is an insufficient pin pressure applied during the welding process [35, 36]. Analyzing the macroscopic test results obtained in this study, a discernible trend emerges: as the welding speed in DAFSW increases, both tunnel and kissing bond defects exhibit larger dimensions. This relationship is directly linked to the heat input during the welding process, with higher welding speeds resulting in reduced heat input. Consequently, this reduced heat input contributes to the enlargement of tunnel and kissing bond defects.

It's interesting that macrostructural observations show no signs of the porosity defects. Porosity is a common issue in aluminum fusion welding. It happens because gases dissolved in the molten metal become trapped when the metal solidifies. To avoid porosity in aluminum welding, the key is to prevent gas from dissolving into the aluminum metal. This can only be accomplished by welding aluminum in its solid state. Friction stir welding is one solid-state welding process that can be used to join aluminum structures. Double-Acting Friction Stir Welding (DA-FSW) is a variation of friction stir welding (FSW) that addresses the issue of porosity defects in aluminum welding by employing a unique technique. In DAFSW, two rotating tools are used instead of one. These tools rotate in opposite directions and are designed to create a more efficient material flow during the welding process. This dual-rotation mechanism helps in several ways to reduce or eliminate porosity defects: (1) the dual-rotation action enhances material mixing in the weld zone. As the two tools rotate in opposite directions, they generate a complex material flow pattern, which helps in dispersing and evacuating trapped gases more effectively. This reduces the likelihood of porosity formation in the weld. (2) the agitation caused by the dual-rotation action aids in the expulsion of gases from the weld zone. This is particularly beneficial for materials like aluminum, which are prone to trapping gases during traditional welding processes. (3) DA-FSW ensures a more uniform distribution of heat throughout the weld zone. This helps in maintaining optimal welding conditions and reduces the formation of voids due to uneven heating.

The Base Material (BM) region presents a grain structure that remains largely undisturbed by the welding procedure. Notably, a variance in the microstructure is evident between the edges and the center of the BM, a disparity stemming from specific treatments administered to the specimen, including processes like extrusion and quenching. Extrusion serves a pivotal role in sculpting a specimen profile devoid of precipitates. The phenomenon of precipitate disappearance can be attributed to the fact that phases prone to precipitation undergo dissolution during the extrusion's pre-heating phase and continue to do so during the extrusion process itself [37]. This dissolution process is accelerated by elevated temperatures combined with the pressure exerted on the specimen [38, 39]. Subsequent to the extrusion, the specimen undergoes a cooling phase. A notable observation here is the more rapid cooling rate at the specimen's edge compared to its center. The edge, being in direct contact with the cooling etchant and ambient air, experiences a quicker drop in temperature. This accelerated cooling rate culminates in a more compact grain structure at the edge, which in turn augments the hardness and resilience of that specific region [40]. Figure 8 offers a visual representation, showcasing the macro and micro structures characteristic of the base metal (BM).

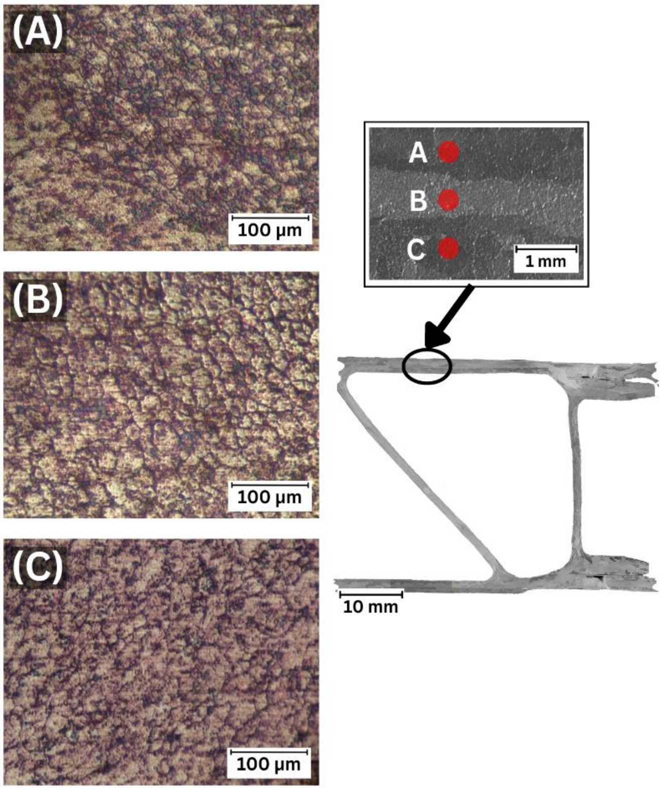

Figure 8. Macro and microstructure of Base Metal (extruded aluminum AA6061 hollow panel)

3.3. Tensile Strength Analysis

The unique curved shape of the specimens concentrates the tensile force primarily within the welded joint area. Figure 9-a visually presents specimens equipped with backed support, while Figure 9-b illustrates the distribution of forces acting on the aluminum hollow panel during tensile testing. After conducting tensile tests and carefully examining the specimens, it becomes evident that fractures consistently occur within the welded joint area for all specimens. These fractures stem from defects within the welding area, which serve as initiation points for cracks when subjected to tensile forces. These initial cracks render the material susceptible to failure within the welded joint area.

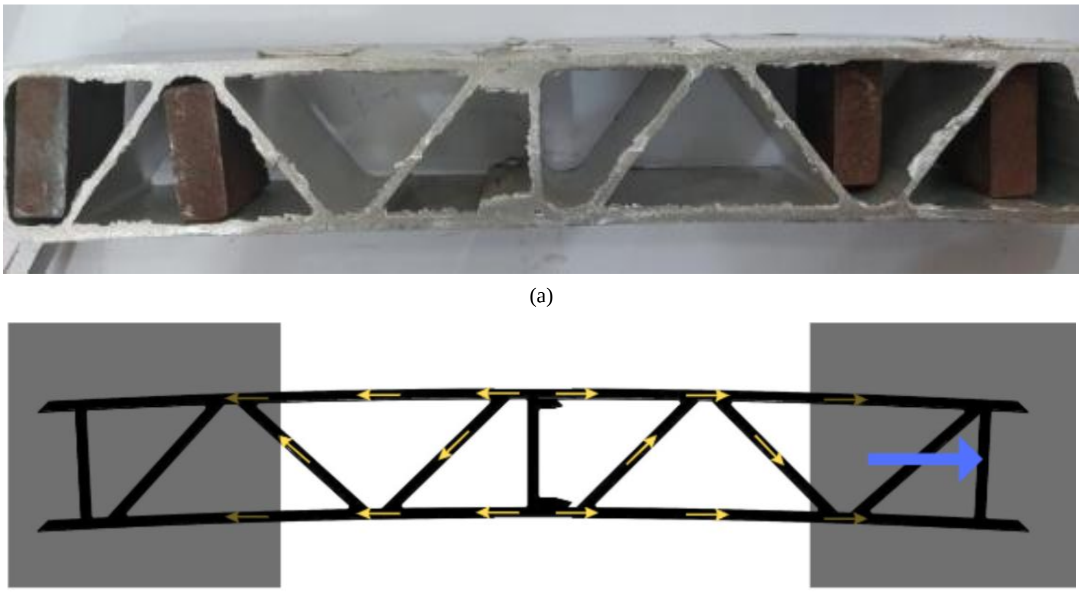

(a)

(b)

Figure 9. Tensile test specimen (a) backed support and (b) forces distribution during tensile test

In this study, the hollow panel specimen represents a segment of a larger curved structure. Consequently, the profile of the hollow panel exhibits a slight curvature in the joint area to seamlessly integrate with the overall structure. During the double-acting friction stir welding (DA-FSW) process, the joint specimen is positioned with a downward curvature. As a result, the bottom tool, operating in the 4G position, welds along the inner curve. Under tensile force, the inner curve experiences stress concentration initially (Figure 10-a), until the joint specimen straightens (Figure 10-b). Once this straightening occurs, the force distributes uniformly across both the upper joint (1G position) and the lower joint (4G position), but the lower joint has experienced fracture (Figure 10-c). In the analysis of tensile testing across all specimens, it was consistently observed that the welded area in the lower joint (4G position) fails first. This initial failure can be solely attributed to the presence of a radius on the lower joint side (4G position), leading to higher stress concentrations during tensile testing. The uneven distribution of stress during testing creates a phenomenon known as eccentricity, where the geometric axis of the test specimen does not perfectly align with the direction of the tensile force. Consequently, when subjected to tensile forces, the curved material initially tends to straighten out, aligning the specimen's axis with the force direction [41, 42]. Figure 10 provides a comprehensive visual representation of the fracture phenomenon observed in the tensile test specimens.

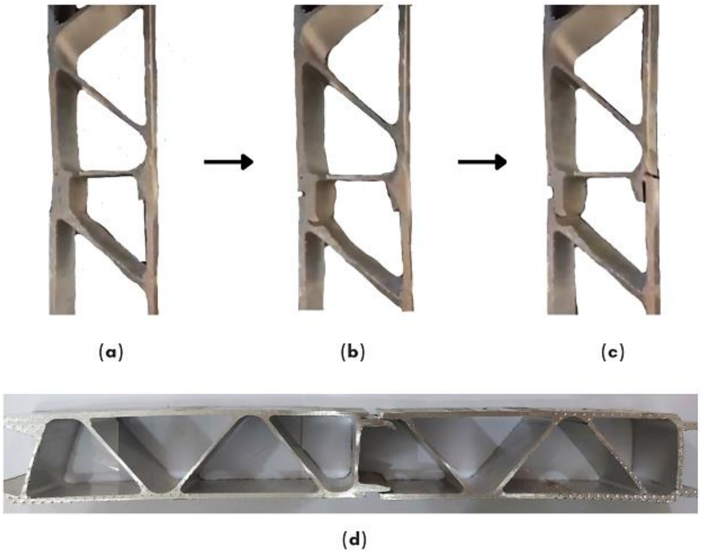

Figure 10. Fracture in tensile test (a) loading start (b) fracture in 4G joint (c) fracture in 1G joint (d) loading finish

To pinpoint the location of the highest stress within the aluminum hollow panel under tensile forces, simulations were conducted using Abaqus software. Figure 11 visually depicts the simulation results of tensile testing on both the 1G and 4G sides. Based on this figure, at the start of the pull, the joint area on the 4G side exhibits a stress contour shifting from light blue (free stress) to light green (low stress), whereas the joint area on the 1G side remains light blue (free stress). This contour variation signifies that stress is predominantly concentrated in the 4G joint area and not uniformly distributed. Consequently, the higher stress levels on the 4G side lead to the material reaching its peak stress level in that area first. This is corroborated by the red contour (high stress) on the 4G side, while the contour on the 1G side retains its orange (medium stress).

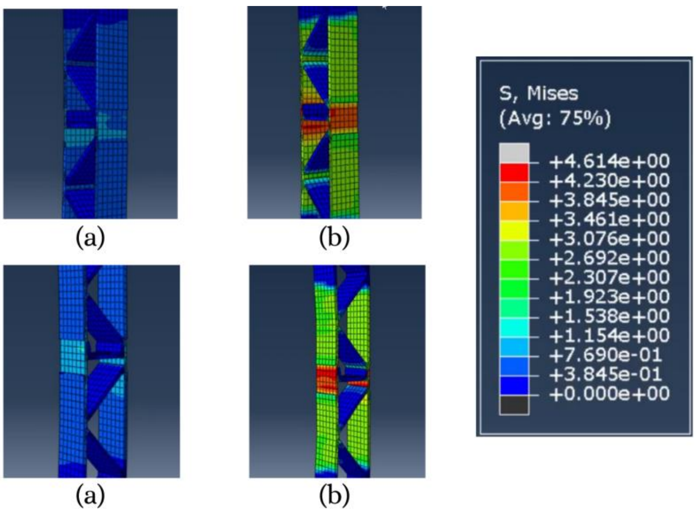

Figure 11. Stress contour in 1G and 4G side during tensile test: (a) initial force (b) maximum force

Tensile testing provides a valuable parameter known as load capacity, which represents the maximum force a structure can endure before experiencing failure. This critical metric serves as a key determinant of a structure's strength, especially when assessing complex-shaped structures for which calculating the cross-sectional area is challenging. In the context of the research on DA-FSW aluminum hollow panel joint testing, a notable observation emerged: joints subjected to a welding speed of 20 mm/min demonstrated superior load capacity compared to those at 40 mm/min, a finding corroborated by Figure 12. The relationship between welding speed and load capacity can be attributed to the phenomenon of increased heat input during the welding process, as outlined in reference [43].

Specifically, a welding speed of 20 mm/min resulted in the highest heat input during welding. Generally speaking, elevated heat input in Friction Stir Welding (FSW) contributes to a more evenly distributed temperature within the joint area. Consequently, this results in a joint that is comparatively softer, better mixed, and facilitates enhanced atomic diffusion between the materials being joined, as explained in reference [44]. Previous studies have suggested an optimal welding speed range of 50-100 mm/min. However, this study reveals that for hollow panels with a thickness of 40 mm and a structure comprising fins and skins due to hollow structure, DA-FSW welding speeds exceeding 40 mm/min fail to create weld joints effectively. This failure arises because the heat generated by the tool is insufficient to soften the workpiece, with the excess heat quickly dissipating to the fin and skin areas due to aluminum's high thermal conductivity. Himawan et al. successfully performed DA-FSW welding at a speed of 30 mm/min, creating high-strength joints when the tool rotation speed reached 1800 rpm [20]. Additionally, this study highlights that FSW welding at speeds below 20 mm/min also fails to create satisfactory joints due to excessive flashing, leading to tunnel-like defects. Furthermore, even if successful, welding at low speeds proves disadvantageous in terms of production cost and time.

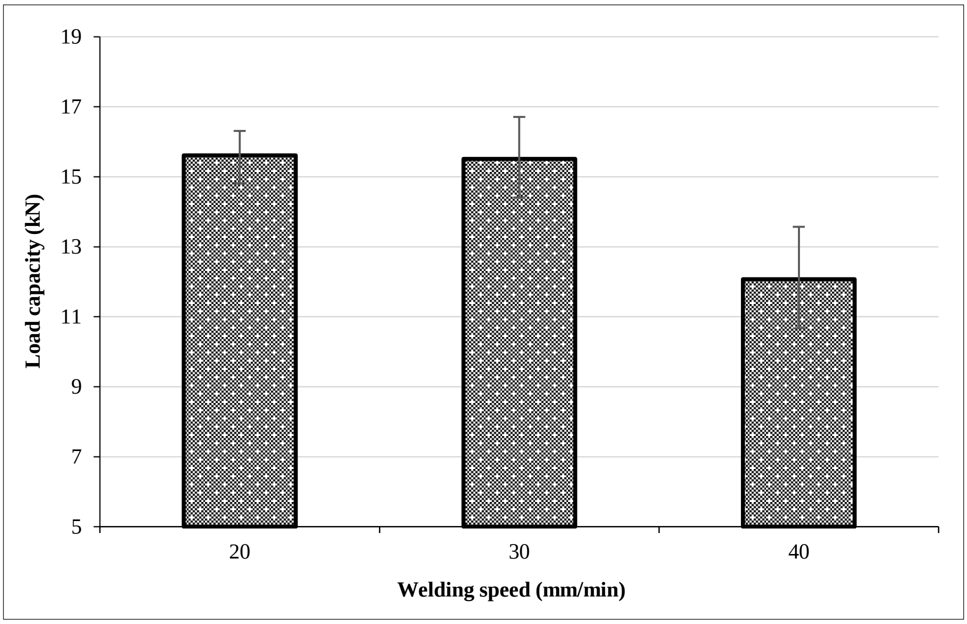

Figure 12. Effect of welding speed on the load capacity of the DAFSW

3.4. Bending Strength Analysis

Where the bending force is applied, it leads to compressive stress, while on the opposite side, tensile stress is generated. Sections experiencing tensile stress are particularly critical as they often serve as the starting point for structural failure [45]. In the context of DAFSW (Double-acting Friction Stir Welding) aluminum hollow panel joints, when they face bending loads, the load gets distributed across all the fins of the structure, as depicted in Figure 13. In this scenario, special attention is directed toward the 1G joint side. The compressive force initiated on the 1G side propagates throughout the entire structure, including the 4G joint side. As the compressive force on the 1G side increases, so does the tensile force experienced at the 4G joint side, eventually reaching its maximum stress level just before failure occurs. The strength of the 4G welding side directly influences the force magnitude distributed to the profile fins, ultimately leading to more significant deformation in the hollow panel's fins when it possesses higher strength.

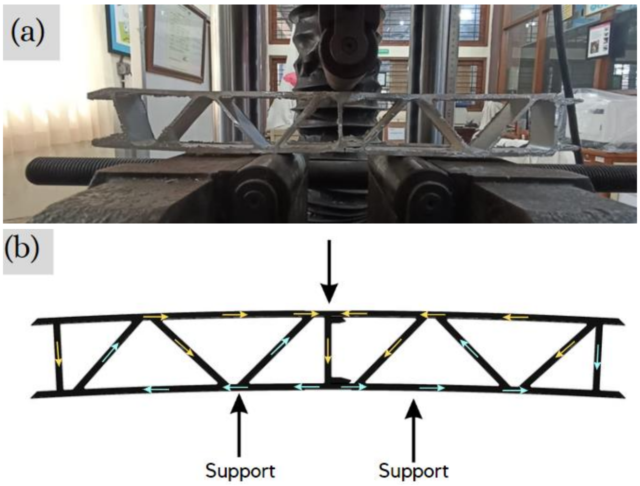

Figure 13. Bending test of hollow panel: (a) loading system, (b) forces distribution

Figure 14 offers a visual representation of the loading process during the bending test and the corresponding response of the test specimen to the applied bending load. To gain deeper insights, stress simulations, and analyses using Abaqus were employed to pinpoint the locations of the highest stress points in the hollow panel structure due to the bending load. Initially, during the application of the bending load, the highest stress emerges at the 1G joint side, vividly depicted by the green contours, while other areas remain relatively stress-free, indicated by the blue contours. However, as the bending load intensifies, stress spreads across the entire profile of the specimen, including the 4G joint side. Tensile stress on the 4G joint side increases in tandem with the compressive force from the former. This is substantiated by the green contours deepening on the 4G joint side, whereas other areas largely maintain their blue contours (indicating low stress). The escalating tensile stress concentration on the 4G joint side culminates in this area being the first to experience cracking. This stress analysis during the bending process in the aluminum hollow panel structure is illustrated in Figure 15.

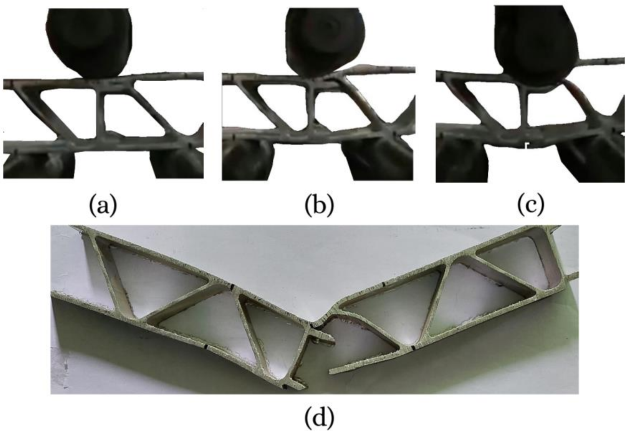

Figure 14. Loading history in bending test (a) initial loading (b) compressive stress in upper side-tensile stress in lower side (c) fractured in lower side (d) fractured in the end of the test

In addition to stress analysis, bending tests provide valuable quantitative data, including bending strength, which signifies the maximum stress a material can endure before experiencing maximum deformation or failure [46]. Figure 16 illustrates the bending strength of DAFSW joints at different welding speeds. Notably, joints welded at a speed of 20 mm/min demonstrate the highest bending strength, reaching 5.47 MPa. Conversely, structures joined using DAFSW at a faster welding speed of 40 mm/min exhibit the lowest bending strength, measuring at 4.86 MPa. This data highlights a clear relationship between welding speed in DAFSW and the bending strength of welded joints in hollow panel structures, with lower welding speeds correlating with higher bending strength. This trend aligns with the results of the tensile tests. Furthermore, Figure 17 enhances this analysis by depicting the increased severity of damage to the fin structures with higher bending strength of joints Figure 17-a illustrates the fracture mechanism of specimens welded at a welding speed of 20 mm/min. Here, the joint strength is robust enough to withstand the bending load, transferring the load to the fin sections. As the fins gradually fail to endure the increasing load, they deform. Notably, this deformation of the bent specimen does not compromise the integrity of the weld joint. Conversely, the fracture mechanism of specimens welded at a welding speed of 40 mm/min (Figure 17-c) reveals that the weld joint lacks the strength to withstand the bending load, resulting in joint failure without causing deformation to the fins. Bending test specimens welded at a welding speed of 30 mm/min display a combination of joint failure and slight deformation of the fins (Figure 17-b). These findings elucidate the intricate relationship between welding speed, joint strength, and structural integrity in DAFSW joints.

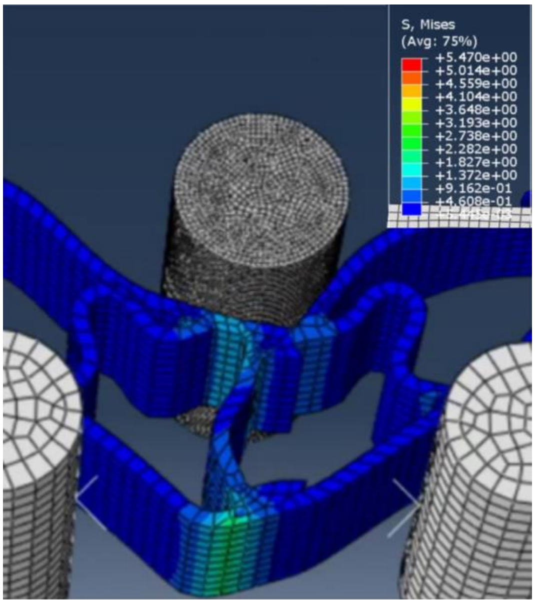

Figure 15. Stress analysis of bending test

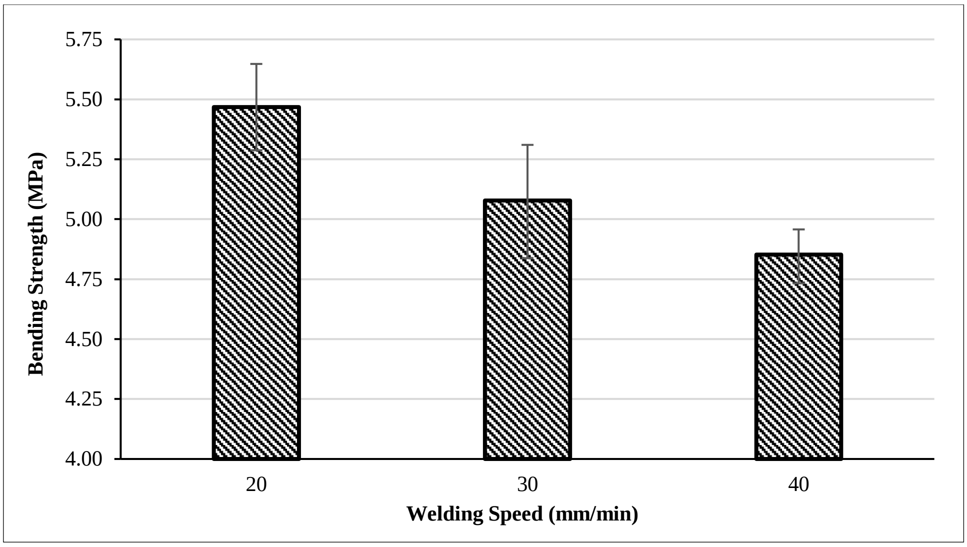

Figure 16. Effect of welding speed on the bending strength of DA-FSW

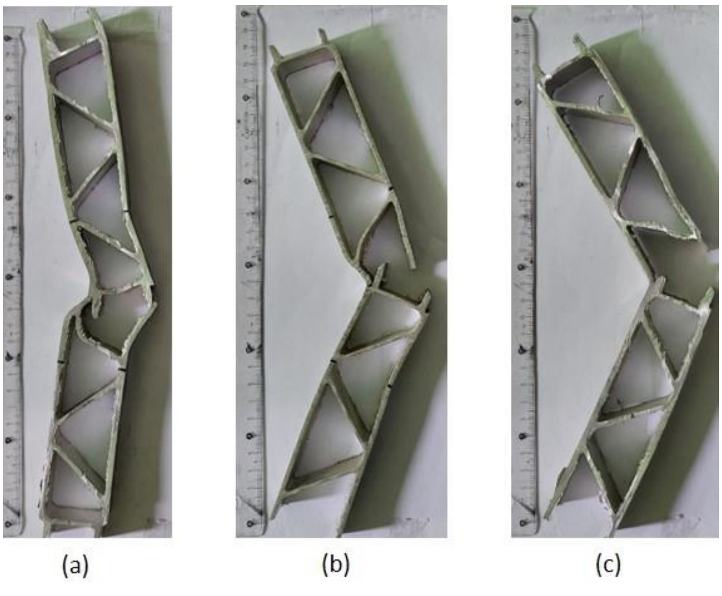

Figure 17. Fracture appearance of bending test (a) 20 mm/min (b) 30 mm/min (c) 40 mm/min

4. Conclusion

The evaluation of welding speed's impact on the quality and characteristics of Double-acting Friction Stir Welding (DA-FSW) joints in aluminum hollow panels has provided valuable insights. Our research reveals that, unlike FSW or DA-FSW welding on solid plates, welding on hollow panels requires slower speeds due to their structure comprising fins and skins. This structure accelerates heat dissipation, necessitating higher heat input. While existing references suggest welding speeds of 50-100 mm/min for solid plates, our study proposes optimal DA-FSW welding of hollow panels at speeds of 20-30 mm/min. This is evident through both macroscopic and microscopic examinations, which reveal consistent grain distribution patterns across welding areas. Specifically, the Stir Zone (SZ) exhibits the most refined grains due to grain recrystallization. In contrast, the Thermo-Mechanically Affected Zone (TMAZ) and Heat Affected Zone (HAZ) show coarser grains, influenced respectively by thermal effects and a lack of exposure to frictional forces.

Tensile testing and stress analysis consistently reveal fractures within the welded joint area, predominantly initiating at the 4G joint side due to higher stress concentrations. This underscores the critical role of welding speed in determining joint integrity and structural performance. Simulation results further emphasize the significance of welding speed, showing a direct correlation with load capacity. Lower welding speeds are found to enhance load capacity by facilitating increased heat input and more effective material mixing during the welding process. Moreover, bending tests establish a clear relationship between welding speed and bending strength, with lower welding speeds demonstrating higher bending strength. Stress analysis conducted during bending tests provides additional insights, illustrating how stress concentrations on the 4G joint side contribute to cracking, particularly affecting the structural integrity of the fins. These findings underscore the importance of optimizing welding parameters, particularly speed, to ensure the structural robustness and durability of welded aluminum hollow panels.

5. Declarations

5.1. Author Contributions

Conceptualization, T. and N.M.; methodology, M.B.U.; software, E.P.B. and A.R.P.; formal analysis, Y.P.D.S.D.; investigation, M.B.U.; resources, M.B.U. and Y.P.D.S.D.; data curation, M.B.U. and Y.P.D.S.D.; writing—original draft preparation, M.B.U.; writing—review and editing, T.; visualization, E.D.W.S.P.; supervision, E.D.W.S.P.; project administration, E.D.W.S.P.; funding acquisition, T. All authors have read and agreed to the published version of the manuscript.

5.2. Data Availability Statement

Data sharing is not applicable to this article.

5.3. Funding and Acknowledgements

This research would like to thank the support of Universitas Sebelas Maret, Lembaga Pengelola Dana Pendidikan, and Badan Riset dan Inovasi Nasional, Indonesia, for providing many facilities and financial support through the RIIM 2022 grant (contract No. 1562.1/UN27.22/HK.07.00/2022), Mandatory Research Grant 2023 (contract No. 228/UN27.22/PT.01.03/2023) and all students in the METALS research group for assisting this research.

5.4. Conflicts of Interest

The authors declare no conflict of interest.

6. References

[1] Georgantzia, E., Gkantou, M., Kamaris, G. S., & Kansara, K. D. (2022). Design of aluminium alloy channel sections under minor axis bending. Thin-Walled Structures, 174. doi:10.1016/j.tws.2022.109098.

[2] Kale, V. N., Rajesh, J., Maiyalagan, T., Lee, C. W., & Gnanamuthu, R. M. (2022). Fabrication of Ni–Mg–Ag alloy electrodeposited material on the aluminium surface using anodizing technique and their enhanced corrosion resistance for engineering application. Materials Chemistry and Physics, 282, 125900. doi:10.1016/j.matchemphys.2022.125900.

[3] Ardika, R. D., Triyono, T., Muhayat, N., & Triyono. (2021). A review porosity in aluminum welding. Procedia Structural Integrity, 33(C), 171–180. doi:10.1016/j.prostr.2021.10.021.

[4] Zhao, C., Ma, J., & Du, S. (2019). The mechanical behaviour of new long-span hollow-core roofs based on aluminum alloy honeycomb panels. Materiali in Tehnologije, 53(3), 311–318. doi:10.17222/mit.2018.075.

[5] Li, S., Dong, H., Wang, X., Liu, Z., Tan, Z., Shangguan, L., Lu, Q., & Zhong, S. (2020). Effect of repair welding on microstructure and mechanical properties of 7N01 aluminum alloy MIG welded joint. Journal of Manufacturing Processes, 54, 80–88. doi:10.1016/j.jmapro.2020.03.009.

[6] Komarasamy, M., Smith, C., Darsell, J., Choi, W., Jana, S., & Grant, G. (2021). Microstructure and mechanical properties of friction stir welded Haynes 282. Materials Characterization, 182, 1–8. doi:10.1016/j.matchar.2021.111558.

[7] Dehghani, M., Amadeh, A., & Akbari Mousavi, S. A. A. (2013). Investigations on the effects of friction stir welding parameters on intermetallic and defect formation in joining aluminum alloy to mild steel. Materials and Design, 49, 433–441. doi:10.1016/j.matdes.2013.01.013.

[8] Liu, Q., Ni, D., Wang, W., Xiang, Y., Han, P., Zhang, T., Qiao, K., Qiang, F., Wang, L., & Wang, K. (2023). Improved mechanical properties of magnesium alloy thick plate joint via uniform microstructure by differential double-shoulder friction stir welding. Materials Letters, 338. doi:10.1016/j.matlet.2023.134045.

[9] Liu, Q., Wang, W., Zhang, T., Ma, Q., Han, P., Ni, D., Qiao, K., & Wang, K. (2024). Low-cycle fatigue behaviour of magnesium alloy thick plate joints fabricated via differential double-shoulder friction stir welding. International Journal of Fatigue, 183. doi:10.1016/j.ijfatigue.2024.108264.

[10] Liu, Q., Wang, W., Peng, P., Zhang, T., Han, P., Guan, X., Wang, Z., Qiao, K., Cai, J., & Wang, K. (2023). Microstructure evolution and strengthening mechanism of friction stir welded joint of 20 mm-thick AZ31 magnesium alloy. Transactions of Nonferrous Metals Society of China, 33(11), 3295–3308. doi:10.1016/s1003-6326(23)66334-4.

[11] Xu, W., Wang, H., Luo, Y., Li, W., & Fu, M. W. (2018). Mechanical behavior of 7085-T7452 aluminum alloy thick plate joint produced by double-sided friction stir welding: Effect of welding parameters and strain rates. Journal of Manufacturing Processes, 35, 261–270. doi:10.1016/j.jmapro.2018.07.028.

[12] Marichamy, M., & Babu, S. (2021). The selection of optimum process parameters on A319 aluminum alloy in friction stir welding MCDM method. Materials Today: Proceedings, 37, 228–231. doi:10.1016/j.matpr.2020.05.080.

[13] Sahu, S. K., Mishra, D., Mahto, R. P., Sharma, V. M., Pal, S. K., Pal, K., Banerjee, S., & Dash, P. (2018). Friction stir welding of polypropylene sheet. Engineering Science and Technology, an International Journal, 21(2), 245–254. doi:10.1016/j.jestch.2018.03.002.

[14] Dewangan, S. K., Tripathi, M. K., & Manoj, M. K. (2019). Effect of welding speeds on microstructure and mechanical properties of dissimilar friction stir welding of AA7075 and AA5083 alloy. Materials Today: Proceedings, 27, 2713–2717. doi:10.1016/j.matpr.2019.12.190.

[15] Liu, H. J., Hou, J. C., & Guo, H. (2013). Effect of welding speed on microstructure and mechanical properties of self-reacting friction stir welded 6061-T6 aluminum alloy. Materials and Design, 50, 872–878. doi:10.1016/j.matdes.2013.03.105.

[16] Haribalaji, V., Boopathi, S., & Asif, M. M. (2021). Optimization of friction stir welding process to join dissimilar AA2014 and AA7075 aluminum alloys. Materials Today: Proceedings, 50, 2227–2234. doi:10.1016/j.matpr.2021.09.499.

[17] Hendrato, Jamasri, Triyono, & Puspitasari, P. (2022). Mechanical Properties and Microstructure Evolution of Double-Sided Friction Stir Welding AA6061-T6. Key Engineering Materials, 935, 73–81. doi:10.4028/p-08610s.

[18] Hendrato, Puspitasari, P., Jamasri, & Triyono. (2024). Fatigue crack growth rate and mechanical properties of one-step double-side friction stir welded AA6061-T6. Results in Engineering, 21. doi:10.1016/j.rineng.2024.101958.

[19] Priyasudana, D., Crisdion, S. A., Puspitasari, P., Triyono, Jamasri, Andoko, & Pramono, D. D. (2023). Double side friction stir welding effect on mechanical properties and corrosion rate of aluminum alloy AA6061. Heliyon, 9(2). doi:10.1016/j.heliyon.2023.e13366.

[20] Hilmawan, M. I., Putri, E. D. W. S., Muhayat, N., Manurung, Y. H. P., Ilhamdi, Sulardjaka, Hendrato, & Triyono. (2024). Effect of tools rotational speed on the mechanical properties of one-step double-acting friction stir welded aluminum alloy AA 6061 hollow panel. International Journal of Lightweight Materials and Manufacture, 7(3), 467–479. doi:10.1016/j.ijlmm.2024.02.002.

[21] Yu, Y., Wang, P., Pei, X., Dong, P., & Fang, H. (2020). Fatigue resistance characterization of frictions stir welds between complex aluminum extrusions: An experimental and finite element study. International Journal of Fatigue, 141, 1–14. doi:10.1016/j.ijfatigue.2020.105861.

[22] Ye, Y., Li, W., & Guo, Z. X. (2020). Performance of concrete-filled stainless steel tubes subjected to tension: Experimental investigation. Thin-Walled Structures, 148, 1–15,. doi:10.1016/j.tws.2020.106602.

[23] Das, D., Bag, S., Pal, S., & Sharma, A. (2023). Material Defects in Friction Stir Welding through Thermo–Mechanical Simulation: Dissimilar Materials with Tool Wear Consideration. Materials, 16(1), 1–20. doi:10.3390/ma16010301.

[24] Ranjan, R., Khan, A. R., Parikh, C., Jain, R., Mahto, R. P., Pal, S., Pal, S. K., & Chakravarty, D. (2016). Classification and identification of surface defects in friction stir welding: An image processing approach. Journal of Manufacturing Processes, 22, 237–253. doi:10.1016/j.jmapro.2016.03.009.

[25] Mahto, R. P., Kumar, R., & Pal, S. K. (2020). Characterizations of weld defects, intermetallic compounds and mechanical properties of friction stir lap welded dissimilar alloys. Materials Characterization, 160, 110115. doi:10.1016/j.matchar.2019.110115.

[26] Dialami, N., Cervera, M., & Chiumenti, M. (2020). Defect formation and material flow in Friction Stir Welding. European Journal of Mechanics - A/Solids, 80, 103912. doi:10.1016/j.euromechsol.2019.103912.

[27] Reimann, M., Goebel, J., Gartner, T. M., & dos Santos, J. F. (2017). Refilling termination hole in AA 2198–T851 by refill friction stir spot welding. Journal of Materials Processing Technology, 245, 157–166. doi:10.1016/j.jmatprotec.2017.02.025.

[28] Yuan, X., Zhang, Z., Gao, Q., Zhou, L., Song, K., Zou, X., Sopu, D., Hu, L., Sun, B., & Eckert, J. (2022). Enhanced mechanical properties of Zr65Cu15Ni10Al10bulk metallic glass by simultaneously introducing surface grooves and multiple shear bands. Journal of Materials Research and Technology, 21, 1490–1506. doi:10.1016/j.jmrt.2022.09.117.

[29] Prabha, K. A., Putha, P. K., & Prasad, B. S. (2018). Effect of tool rotational speed on mechanical properties of aluminium alloy 5083 weldments in friction stir welding. Materials Today: Proceedings, 5(9), 18535–18543. doi:10.1016/j.matpr.2018.06.196.

[30] Qian, J., Li, J., Sun, F., Xiong, J., Zhang, F., & Lin, X. (2013). An analytical model to optimize rotation speed and travel speed of friction stir welding for defect-free joints. Scripta Materialia, 68(3–4), 175–178. doi:10.1016/j.scriptamat.2012.10.008.

[31] Khan, N. Z., Siddiquee, A. N., Khan, Z. A., & Shihab, S. K. (2015). Investigations on tunneling and kissing bond defects in FSW joints for dissimilar aluminum alloys. Journal of Alloys and Compounds, 648, 360–367. doi:10.1016/j.jallcom.2015.06.246.

[32] Zettler, R., Vugrin, T., & Schmücker, M. (2010). Effects and defects of friction stir welds. Friction Stir Welding, 245–276, Woodhead Publishing, Sawston, United Kingdom. doi:10.1533/9781845697716.2.245.

[33] Ahmed, M. M. Z., Wynne, B. P., Rainforth, W. M., & Threadgill, P. L. (2012). Microstructure, crystallographic texture and mechanical properties of friction stir welded AA2017A. Materials Characterization, 64, 107–117. doi:10.1016/j.matchar.2011.12.005.

[34] Sato, Y. S., Takauchi, H., Park, S. H. C., & Kokawa, H. (2005). Characteristics of the kissing-bond in friction stir welded Al alloy 1050. Materials Science and Engineering: A, 405(1–2), 333–338. doi:10.1016/j.msea.2005.06.008.

[35] Essa, G. M. F., Zakria, H. M., Mahmoud, T. S., & Khalifa, T. A. (2018). Microstructure examination and microhardness of friction stir welded joint of (AA7020-O) after PWHT. HBRC Journal, 14(1), 22–28. doi:10.1016/j.hbrcj.2015.05.002.

[36] Kadlec, M., Růžek, R., & Nováková, L. (2015). Mechanical behaviour of AA 7475 friction stir welds with the kissing bond defect. International Journal of Fatigue, 74, 7–19. doi:10.1016/j.ijfatigue.2014.12.011.

[37] Priya, P., Johnson, D. R., & Krane, M. J. M. (2017). Precipitation during cooling of 7XXX aluminum alloys. Computational Materials Science, 139, 273–284. doi:10.1016/j.commatsci.2017.08.008.

[38] Jung, B. B., Lee, H. K., & Park, H. C. (2013). Effect of grain size on the indentation hardness for polycrystalline materials by the modified strain gradient theory. International Journal of Solids and Structures, 50(18), 2719–2724. doi:10.1016/j.ijsolstr.2013.05.002.

[39] Wang, Y., Zhao, G., Sun, L., Wang, X., Lv, Z., & Sun, Y. (2023). Effects of billet heating temperature and extrusion speed on the microstructures and mechanical properties of the longitudinal welds in aluminum alloy profiles with complex cross-section. Vacuum, 207, 1–15. doi:10.1016/j.vacuum.2022.111578.

[40] Jo, H., Kang, M., Park, G. W., Kim, B. J., Choi, C. Y., Park, H. S., Shin, S., Lee, W., Ahn, Y. S., & Jeon, J. B. (2020). Effects of cooling rate during quenching and tempering conditions on microstructures and mechanical properties of carbon steel flange. Materials, 13(18), 1–16. doi:10.3390/MA13184186.

[41] Nitu, E. L., Diakhaté, M., Bădulescu, C., Grédiac, M., Blaysat, B., Iordache, D. M., Bosneag, A., Adrien, J., Maire, E., Dhondt, M., & Demmouche, Y. (2022). Analyzing defects and their effects on the strength of a three-layer FSW joint by using X-ray microtomography, localized spectrum analysis, and acoustic emission. Materials Characterization, 190, 1–20. doi:10.1016/j.matchar.2022.112069.

[42] Charpentier, J. B., Perderiset, C., Bouvard, J. L., Georgi, F., Pino-Muñoz, D., & Rasselet, F. (2021). On the influence of eccentricity on Thick Adherend Shear Tests. International Journal of Adhesion and Adhesives, 110, 1–11. doi:10.1016/j.ijadhadh.2021.102910.

[43] Kubit, A., Trzepieciński, T., Gadalińska, E., Slota, J., & Bochnowski, W. (2021). Investigation into the effect of rfssw parameters on tensile shear fracture load of 7075-t6 alclad aluminium alloy joints. Materials, 14(12), 1–28. doi:10.3390/ma14123397.

[44] Kubit, A., Trzepieciński, T., Kluz, R., Ochałek, K., & Slota, J. (2022). Multi-Criteria Optimisation of Friction Stir Welding Parameters for EN AW-2024-T3 Aluminium Alloy Joints. Materials, 15(15), 1–28. doi:10.3390/ma15155428.

[45] Jia, X., Hao, K., Luo, Z., & Fan, Z. (2022). Plastic Deformation Behavior of Metal Materials: A Review of Constitutive Models. Metals, 12(12), 1–33. doi:10.3390/met12122077.

[46] Sahu, P. K., & Pal, S. (2017). Mechanical properties of dissimilar thickness aluminium alloy weld by single/double pass FSW. Journal of Materials Processing Technology, 243, 442–455. doi:10.1016/j.jmatprotec.2017.01.009.